Phenothiazine-based theranostic compounds for in vivo near-infared fluorescence imaging of β-amyloid plaques and inhibition of Aβ aggregation

Yongliang Li, Jing Cai, Longjia Yan, Wanzheng Zhang, Li Li, Zhiyun Du, Yanxiong Fang, Changzhi Dong, B. Meunier, Huixiong Chen

Version of Record: https://www.sciencedirect.com/science/article/pii/S0143720819311982
Manuscript_a74f6512092559daadd67dc8d5a0be15

Phenothiazine-based theranostic compounds for in vivo near-infared fluorescence imaging of β-amyloid plaques and inhibition of Aβ aggregation

YongLiang Li,[1, //] Jing Cai,[3, //] Longjia Yan,[1, //] Wanzheng Zhang,[1] Ii Li,[3] Zhiyun Du,[1] YanXiong Fang,[1] ChangZhi Dong,[1, 4] Bernard Meunier,[1, 5] Huixiong Chen,[1,2, ✉]

1. Faculty of Light Industry and Chemical Engineering, Guangdong University of Technology, Guangdong, 510006, China;
2. CNRS, UMR8601, Laboratoire de Chimie et Biochimie Pharmacologiques et Toxicologiques, CBNIT, Université Paris Descartes, PRES Sorbonne Paris Cité, UFR Biomédicale, 75006 Paris, France;
3. Imaging Diagnosis and Interventional Center, State Key Laboratory of Oncology in South China, Sun Yat-sen University Cancer Center, Guangzhou, Guangdong 510060, China
4. Université Paris Diderot, Sorbonne Paris Cité, ITODYS, UMR 7086 CNRS, 75013 Paris, France;
5. Laboratoire de Chimie de Coordination du CNRS, 205 Route de Narbonne, 31077 Toulouse Cedex, France.

✉ Corresponding author: Huixiong Chen, UFR Biomédicale, Université Paris Descartes, Tel: (+33)142864085, Email: huixiong.chen@parisdescartes.fr

Abstract: A global burden of Alzheimer's disease (AD) has been growing over last decades. Evidence indicates that β-amyloid (Aβ) production and senile plaque deposition in the brain is causative in the onset of AD pathogenesis. It appears much earlier than cognitive decline and plays a key role in initiating and developing AD neuropathology. As such, there is an intense passion with discovering theranostic agents which make a significant impact in diagnostic and therapy. Herein, we report an investigation of novel phenothiazine-based compounds as promising potential theranostic agents for AD. Remarkably, they have exhibited a high binding affinity toward Aβ aggregates, a good biostability and a strong increase in their fluorescence intensity with blue shift when interacting with Aβ aggregates. Furthermore, they have been simultaneously applied to perform NIR in vivo imaging of β-amyloid plaques in double transgenic AD mouse model, to prevent self-aggregation of Aβ monomer from forming toxic oligmers and to reduce Aβ-induced toxicity of human neuroblastoma cells (SH-SY5Y).

Keywords: Theranostic agents, Near-infrared fluorescence imaging, Inhibitors, Alzheimer's disease

1. Introduction

Alzheimer's disease (AD) is chronic neurodegenerative disorders, which are principally characterized by synaptic dysfunction, neuronal atrophy, progressive memory impairment and

cognitive decline. There is an accelerating worldwide effort under way to find disease-modifying therapies to postpone its onset and prevent it from progression. Nevertheless, none of the clinically tested drugs have shown significant effectiveness up to now.[1-3] The unsuccess of many drug candidates into clinical application might be attributed to their treatment at an advanced stage, which has already resulted in severe irreversible injury in the brain. Therefore, it is very desirable to find safe and effective therapeutics as well as imaging probes for early diagnosis and assisting drug development.

The amyloid hypothesis, which suggests that β-amyloid (Aβ) production and senile plaque deposition in the brain is causative in the onset of AD pathogenesis, is widely accepted and has gained adequate attention for AD drug development.[4-5] Aβ selectively builds up in the mitochondria in the cells of Alzheimer's-affected brains,[6] which can further transform into non-toxic aggregated species through several forms of flexible soluble oligomers or protofibrils.[7-8] Recent studies suggest that oligomeric soluble Aβ is mainly responsible for AD pathogenesis, and its levels are more important in the progression of the disease.[9] Indeed, the soluble Aβ oligomers can induce tau to misfold and result in pathological hyperphosphorylation of tau, leading to microtubule disruption and degenerative neuritis.[10] They can directly induce neuronal hyperploidy followed by synaptic failure and bring about the neuronal death in the cerebral cortex, which are responsible for AD initiation and progression.[11-13] They can also generate oxidative stress, neuroinflammation and abnormalities in calcium (Ca2+) homeostasis.[14-16] Furthermore, amyloid senile plaques appear much earlier than cognitive dysfunction and play a key role in the onset of AD neuropathologic events,[17-18] suggesting that these abnormal protein deposits inside brain represent a good predictive biomarker for diagnosis and also an important therapeutic target of AD.[19-21]

Recent advances in optical imaging technologies, which make a significant impact in diagnostic and interventional imaging over the next decade,[22] have driven the development of fluorescent probes into a rapidly expanding era. Moreover, modern and efficient optical imaging systems such as fluorescence molecular tomography (FMT) imaging and the hydrid technique known as FMT-CT imaging have enabled the visualization and quantification of disease progression using near-infrared (NIR) fluorophores, which provide sufficient light propagation into deeper tissue and avoid auto-fluorescence from biological matter.[23] Although many NIR fluorophores have been designed and used for AD imaging in vivo,[24-27] it is not easy for NIR probes to meet the diverse and rigorous imaging conditions for oligomeric and

fibrillar species of β-amyloid, such as good blood–brain barrier permeability, high binding affinity, high selectivity and low neurotoxicity. Moreover, very few of NIR probes used as theranostic agents have been reported.

Theranostics is emerging as a promising therapeutic paradigm that integrates both of therapeutics and diagnostics, in order to monitor the response to treatment and improve safety and efficacy of drug. Several distinct advantages are attractive for theranostic agents due to their intrinsic ability to provide imaging with significant biodistribution and pharmacokinetic information about the exact target compound before, during, and after therapy. We have previously shown that phenothiazine-based compounds could be used as dual inhibitors and probes of β-amyloid fibrillogenesis.[30] One of these compounds, 4a1 could effectively inhibit the formation of amyloid fibrils by Aβ and disaggregate its preformed amyloid fibrils. We speculated that the turn-on and blue-shift fluorescence emission of this type of probes might be obtained probably due to their intercalation into the hydrophobic clefs oriented parallel to the main fibril axis formed by the nonpolar residues Val18 and Phe20 on the surface of Aβ fiber. Indeed, based on the results of the docking simulations, the phenothiazine ring scaffold of compound 4a1 was preferentially buried into the hydrophobic binding pocket (Figures S8 and S9), which could produce strong π–π stacking and hydrophobic–hydrophobic interactions with Aβ protein. This was also confirmed by a striking improvement in the binding energies to Aβ fibrils. However, the poor solubility of these compounds have impeded their application in NIR imaging *in vivo*. Herein, we attempt to investigate whether structural alterations at its periphery by the water solubilizing groups (Scheme 1) can affect the binding and fluorescent properties, as well as Aβ-inhibiting and neuroprotective ability of these probes.

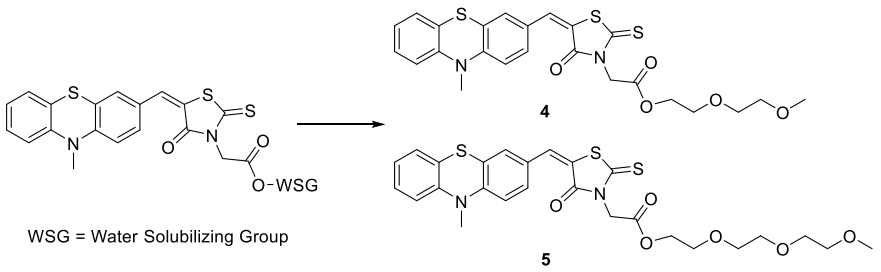

Figure 1: Chemical structure of Phenothiazine-based theranostic compounds **4** and **5**

2. Experimental

2.1 *Materials and measurements*

All commercially available chemicals and solvents were used as received. ^{1}H NMR and ^{13}C NMR spectra were obtained respectively, on 400 MHz spectrometer in $CDCl_3$ or DMSO-d6, and the chemical shift (δ) was quoted in δ values (ppm) relative to TMS as internal standard. MS (ESI) was measured by using a QTRAP instrument with ion source. Elemental analysis was performed for the purity of the final products (> 95%). Fluorescence was evaluated by a spectrofluorophotometer (RF-5301PC, Shimadzu, Japan).

$A\beta_{1-42}$ was provided by GL Biochem. Transgenic mice (APPswe/PSEN1dE9, 12 months old, male) and male C57BL/6 counterparts, used for in vivo imaging were purchased from GDMLAC (certification number: 44007200000555). All animal test procedures were approved by Sun Yat-sen university animal ethical experimentation Committee.

2.2. Process of probe synthesis

*2.2.1. General Method for the Synthesis of compounds **3***

To a solution of the corresponding alcohol (2.0 mmol, 1 equiv), (4-oxo-2-thioxo-thiazolidin-3-yl)-acetic acid (2.0 mmol, 1 equiv) in 5 mL DCM and DMAP (0.01 mmol, 0.005 equiv) was added at 0°C. Finally, DCC (2.0 mmol, 1 equiv) in 5 mL DCM was added dropwise and the reaction mixture was stirred at at 0°C for 6 hours. The reaction was diluted with 10 mL of DCM and the formed solid was filtered off. The filtrate was dried over anhydrous Na_2SO_4 and the solvents were removed under reduced pressure. The residue was purified by flash chromatography (n-Hexane : EtOAc = 5:1) to give the product.

*(4-Oxo-2-thioxo-thiazolidin-3-yl)-acetic acid 2-(2-methoxy-ethoxy)-ethyl ester (**3a**).* 440 mg (75%). Yellow oil. ^{1}H NMR (400 MHz, $CDCl_3$) δ 4.76 (s, 2H), 4.35 – 4.31 (m, 2H), 4.08 (s, 2H), 3.71 – 3.69 (m, 2H), 3.63 (dd, *J* = 5.6, 3.6 Hz, 2H), 3.55 (dd, *J* = 5.6, 3.6 Hz, 2H), 3.39 (s, 3H). MS (ESI) m/z: 294.1 $[M + H]^+$.

*(4-Oxo-2-thioxo-thiazolidin-3-yl)-acetic acid 2-[2-(2-methoxy-ethoxy)-ethoxy]-ethyl ester (**3b**).* 539 mg (80%). Yellow oil. ^{1}H NMR (400 MHz, $CDCl_3$) δ 4.75 (s, 2H), 4.33 – 4.29 (m, 2H), 4.08 (s, 2H), 3.71 – 3.67 (m, 2H), 3.66 – 3.62 (m, 6H), 3.55 (dd, *J* = 5.6, 3.6 Hz, 2H), 3.37 (s, 3H). MS (ESI) m/z: 338.1 $[M + H]^+$.

*2.2.2. General Method for the Synthesis of compounds **4** and **5**.*

To a round bottom flask containing a solution of 10-methyl-10H-phenothiazine-3-carbaldehyde **2** (0.40 mmol, 1 eq) and corresponding rhodanines **3** (0.44 mmol, 1.1 eq) in 5 mL of THF was added piperidine (0.04 mmol, 0.1 eq) and the mixture was heated at 50 °C for

3 hours. The crude mixture was concentrated under reduced pressure and purified by flash chromatography to give the product.

*[5-(10-Methyl-10H-phenothiazin-3-ylmethylene)-4-oxo-2-thioxo-thiazolidin-3-yl]-acetic acid 2-(2-methoxy-ethoxy)-ethyl ester (**4**).* 169 mg (82%). Red oil. ^{1}H NMR (400 MHz, $CDCl_3$) δ 7.62 (s, 1H), 7.30 (dd, *J* = 8.4, 2.0 Hz, 1H), 7.23 – 7.17 (m, 2H), 7.13 (dd, *J* = 7.6, 1.2 Hz, 1H), 6.98 (td, *J* = 7.6, 1.2 Hz, 1H), 6.84 (d, *J* = 8.4 Hz, 2H), 4.89 (s, 2H), 4.36 – 4.33 (m, 2H), 3.73 – 3.70 (m, 2H), 3.65 – 3.63 (m, 2H), 3.56 – 3.53 (m, 2H), 3.41 (s, 3H), 3.38 (s, 3H). ^{13}C NMR (100 MHz, $CDCl_3$) δ 192.6, 167.0, 166.0, 148.1, 144.1, 133.1, 131.1, 128.9, 127.8, 127.4, 127.3, 124.5, 123.5, 122.2, 119.6, 114.7, 114.3, 71.9, 70.6, 68.9, 65.0, 59.1, 44.8, 35.6. MS (ESI) m/z: 517.1 $[M + H]^+$. Anal. Calcd for $C_{24}H_{24}N_2O_5S_3$: C, 55.80; H, 4.68; N, 5.42. Found: C, 55.69; H, 4.71; N, 5.45.

*[5-(10-Methyl-10H-phenothiazin-3-ylmethylene)-4-oxo-2-thioxo-thiazolidin-3-yl]-acetic acid 2-[2-(2-methoxy-ethoxy)-ethoxy]-ethyl ester (**5**).* 188 mg (84%). Red oil. ^{1}H NMR (400 MHz, $CDCl_3$) δ 7.62 (s, 1H), 7.30 (dd, *J* = 8.4, 2.0 Hz, 1H), 7.22 – 7.17 (m, 2H), 7.13 (dd, *J* = 7.6, 1.2 Hz, 1H), 7.00 – 6.96 (m, 1H), 6.84 (d, *J* = 8.4 Hz, 2H), 4.89 (s, 2H), 4.36 – 4.33 (m, 2H), 3.73 – 3.70 (m, 2H), 3.64 (dd, *J* = 5.6, 3.6 Hz, 2H), 3.55 (dd, *J* = 5.6, 3.6 Hz, 2H), 3.41 (s, 3H), 3.38 (s, 3H). ^{13}C NMR (100 MHz, $CDCl_3$) δ 192.6, 167.0, 166.0, 148.1, 144.1, 133.1, 131.1, 128.9, 127.8, 127.4, 127.3, 124.5, 123.5, 122.3, 119.7, 114.7, 114.3, 71.9, 70.7, 70.6, 70.5, 68.8, 65.0, 59.0, 44.8, 35.7. MS (ESI) m/z: 561.2 $[M + H]^+$. Anal. Calcd for $C_{26}H_{28}N_2O_6S_3$: C, 55.70; H, 5.03; N, 5.00. Found: C, 55.67; H, 5.05; N, 5.02.

2.3. Fluorescence spectral evaluation of probes with $A\beta_{1-42}$ aggregates and BSA

To the solution of probes (0.4 μM) in 10 μL of PBS (pH = 7.4) was added a solution of 10 μL of aggregated $A\beta_{1-42}$ (20 μM) or BSA (180 μg/mL), and incubated for 30 min at RT. Fluorescence excitation/emission wavelength and intensity were measured.

2.4. In vitro binding assays

To obtain the dissociation constants, a solution of $A\beta_{1-42}$ aggregates (0.5 μM in the final assay concentrations) was mixed with various concentrations of probes in PBS (10^{-5} to 10^{-10} M in the final assay concentrations) and incubated at RT with constant shaking for 30 min. The intensity of the fluorescent signal was determined and Kd values were calculated by fitting the data to the single-site ligand binding module in Grafpad Prism.

2.5. The stability of probes in mice plasma

Blood was drawn from normal SD rat (7 weeks, male), and the plasma was separated by centrifugation at 4000 rpm for 10 min and stored at −80 °C. The following procedures were used. To 315 μL of rat plasma or PBS (as a standard sample) was added 35 μL of probe **4** or **5** in ethanol (50 μM), and the mixture was incubated at 37 °C for 30 or 60 min. Then, after 30 or 60 min, the mixture was treated with 350 μL of CH_3CN and separated by centrifugation at 40000 rpm for 5 min. The supernatant were treated by the same method once again. Finally, the supernatant were analyzed by HPLC, and the spectra were recorded using a C_{18} column (4.6 mm × 250 mm) and CH_3CN/H_2O (85:15%) with a flow rate of 1 mL/ min at 30 ℃.

2.6. Ex vivo fluorescence staining of brain sections

Frozen section of brain tissue from double transgenic mice (C57BL/6, APP/PS1, 12 months old, male) and age-matched wild mice (C57BL/6, 12 months old, male) were sacrificed after iv injection with **4** (4 mg/kg, 20% DMSO, 80% propylene glycol, 50 μl), and the brain was excised, embedded in optimum cutting temperature compound, and frozen in dry ice immediately. Fluorescence imaging was carried out by using a fluorescence microscope (Olympus BX63) equipped with GFP and Cy5 filter sets. Next, the same section was costained with ThT to confirm the distribution of Aβ plaques

2.7. In vivo near-infrared imaging

Double transgenic mice (C57BL/6, APP/PS1, 12 months old, male) and age-matched wild mice (C57BL/6, 12 months old, male) were shaved before imaging. The mice were injected intravenously with probe **4** (4 mg/kg, 20% DMSO, 80% propylene glycol, 50μl). Fluorescence imaging were performed at different time points with mice kept under anesthesia with 2.5% isoflurane gas in an oxygen flow. In addition, a filter set (ex. at 500 and em. at 680 nm) was used for the measurement. The optical images were acquired using an exposure time of 1s. Imaging data were analyzed by Living Image software, the region of interest (ROI) was drawn around the brain regions. The relative fluorescence data [F(t)/F(pre)] were analyzed by normalizing the fluorescence intensity to the fluorescence background of each mouse, where F(t) is the fluorescence intensity in the ROI and F(pre) is the fluorescence background signal in the same region.

2.8. Cytotoxicity analysis

SH-SY5Y cells were cultured with F12 (Gibco) and EMEM (ATCC, USA) mixture at a mixing rate of 1:1 contains 10% fetal bovine serum (FBS, Gibco, USA) and 1% Penicillin-Streptomycin solution (Gibco, USA). SH-SY5Y cells were plated onto 96-well plates at a density of 5 x 10^4 cells/mL in cell culture medium and 100 μL suspension per well was added. The cells in each well were treated with various concentrations of probes, respectively, and incubated at 37 ℃ and 5% CO_2 for 24 h.

For the effect of probes on $A\beta_{1-42}$-induced cell toxicity, SH-SY5Y cells were plated onto 96-well plates at a density of 5 x 10^4 cells/mL in cell culture medium and seed 100 μL per well. Probes **4** and **5** of final concentration 0.1 μM or 0.5 μM was applied together with monomeric $A\beta_{(1-42)}$ of concentration 5 μM, and incubated at 37 ℃ for 24 h.

Next, 10 μL of 3-(4,5-dimethylthiazol-2-yl)-2,5-diphenyltetrazolium bromide (MTT) solution (0.5 mg/mL, Sigma, USA) was added and further incubated for 4 h at 37 ℃. The MTT solution was removed and then 150 μL of DMSO was added to each well to dissolve the formazan crystals. The absorbance of each well was determined at 570 nm, using a microplate reader.

2.9. Fluorescence staining of inhibition of self-aggregation in SH-SY5Y cells.

2000 cells per well were seeded in 96 wells plate for 24 h. $A\beta_{1-42}$ monomer (50 μL, 0.5 μM) was mixed with or without probe **4** (50 μL, 0.2 μM or 1 μM), then added into 96 well plate and incubated with cells at 37°C and 5% CO_2 for 48h. All the culture medium was replaced with a fresh medium contains 0.5 μM compound and the cells were cultured for 30 min in incubator. The fluorescence intensity was recorded by fluorescence microscope (Olympus IX71 inverted fluorescence microscope) and calculated by measuring the average of pixel intensity per field through the program Image J. Digital images of four random fields were treated at 10x magnification.

2.10. ADMET and molecular docking studies

Computer aided ADME studies have been done by using CHARMM force field (Discovery Studio 2.5 software, Accerlrys, Inc., San Diego, Calif.). Docking procedures were carried out using Autodock 4.2 software on Aβ fibril structures from RCSB protein Data Bank (PDB ID: 2LMO) according to the Lamarckian genetic algorithm method. Probes were constructed with Sketch and optimized with minimize modular at the Tripos force field[31] and

Gasteiger-Marsili charges theory[32-33] in Sybyl 6.0 software. The segment of 16-KLVFFA-21 of the Aβ fibrils was used as the potential binding site for the probes.[34] A grid of 42, 104 and 84 in x, y and z directions centered on this site was built with a grid spacing of 0.458 Å. The most reliable pose of the ligand was generated from 1200 docking poses. The best poses were analyzed for hydrogen bonding or hydrophobic interaction of the ligands with the Aβ fibrils using AutoDock Tools 1.5.6 and the figures were generated using PyMol 1.8.x software.

3. Results and discussion

3.1. Synthesis of the probes

As shown in Scheme 1, the compound **1** was synthesized by alkylating phenothiazine with methyl iodide in DMF in the presence of NaH and followed by Vilsmeier–Haack reaction in the presence of $POCl_3$ in DMF, to introduce an aldehyde group at the C-3 position of the phenothiazine ring. Then, the aldehyde group was treated by a Knoevenagel condensation with the appropriate rhodanines **3**, prepared from (4-oxo-2-thioxo-thiazolidin-3-yl)-acetic acid and described in Schemes S1 (Supporting Information).

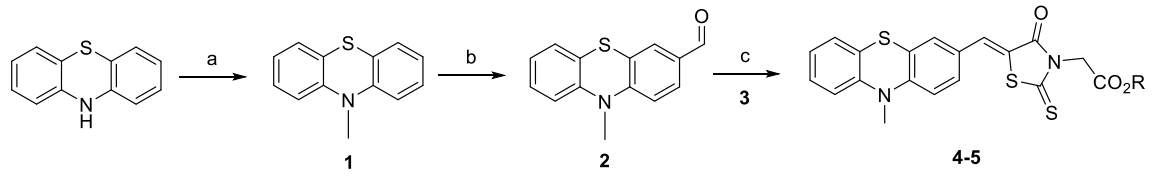

Scheme 1. Conditions and reagents: a) CH_3I, NaH, DMF; b) $POCl_3$, DMF; c) **3**, piperidine, THF.

3.2. Fluorescent properties of the probes

We first evaluated spectroscopic properties of the probes. As shown in Table 1, probes **4** and **5** exhibited emission wavelength of 667-670 nm in PBS, which fell in the range for NIR probes, accompanied with large Stokes shifts, around 128 nm and 187 nm respectively. Moreover, they showed high sensitivity to the solvent polarity (Fig. S1). This is consistent with that observed in the previous study,[30] suggesting that the structural alteration by the water solubilizing group did not affect the binding and fluorescent properties of the probes. The plots of relative fluorescence intensity versus concentration of probes **4** and **5** was then performed to show a linear correlation in the range of 0-10 μM with a coefficient of 0.9975 and 0.9953 respectively (Figure S2).

Table 1. Fluorescent Properties, Binding Data and Calculated log P (clog P) Values of probes **4** and **5**

Probe	λ_{abs}[a](nm)	λ_{em1}[b](nm)	λ_{em2}[b](nm)	Φ (%)[c]	fold[d]	K_d (nM)[e]	log *P*[f]	clog *P*[f]
4	482	670	610	6.1/0.4	69.3	28.2±2	3.03	4.61
5	480	667	605	8.0/0.8	28.3	59.8±6	2.88	4.97

[a]Absorbance (λ_{abs}) measured in PBS. [b]Determined in PBS (λ_{em1}) and upon binding with Aβ aggregates (λ_{em2}). [c]Measured in Aβ/PBS, respectively. [d]Fold increase in fluorescence intensity upon binding with Aβ aggregates. [e]K_d value was measured in triplicate with results given as the mean ± SD. [f]The values were calculated using chemdraw program.

Next, the photostability of these probes (10 mM in DMSO) were also evaluated under UV (254 nm), light and sunlight respectively. The results exhibited that these dyes were stable to continuous irradiation for 12 hours (Figure S3). Probes **4** and **5** have a molecular weight less than 600 Da and their calculated logP values are 3.03 and 2.88 respectively. LogP values of these probes are lower than that of compound 4a (logP = 3.68), suggesting that they have better biocompatibility and penetration of the intact BBB as well as lower nonspecific binding and a more rapid washout rate from the brain.

3.3. In vitro Evaluations

Then, we examined the fluorescent properties of these free probes upon binding toward $A\beta_{1-42}$ aggregates in PBS (pH = 7.4) and in the presence of bovine serum albumin (BSA). As shown in Figure 2, fluorescence intensity and emission wavelength were changed significantly. Indeed, a remarkable enhancement of fluorescence intensity of compounds **4** and **5** (about 69.3-fold for **4** and 28.3-fold for **5**) and the turn-on and blue-shift fluorescence emission (about 60 nm) were observed after incubation with $A\beta_{1-42}$ aggregates in PBS, suggesting that these probes might be intercalated into the hydrophobic pocket of Aβ aggregates, leading to a restrained rotational relaxation.[25] This is further confirmed by the significant enhancement of the fluorescent quantum yield after binding to Aβ aggregates (table 1). On the contrary, a very week interaction was observed with the combination of probes and BSA in PBS (Figure S4).

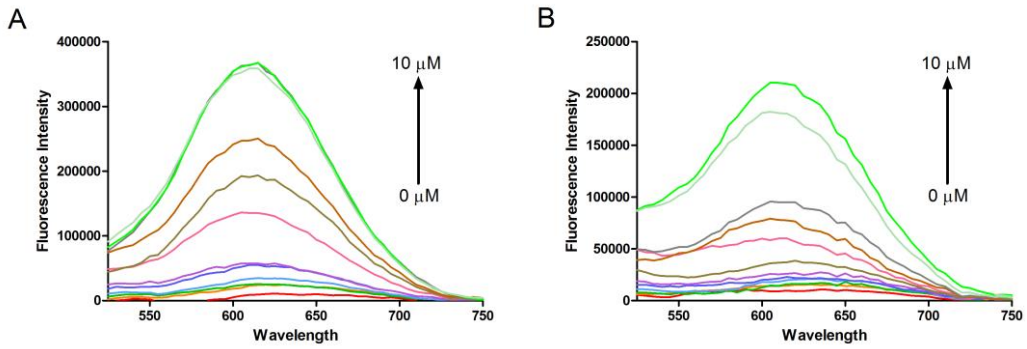

Figure 2. The fluorescence spectroscopic titration of probes **4** (A) or **5** (B) at 0.2 μM by stepwise addition of $A\beta_{1\text{-}42}$ aggregates (from 0 μM to 10.0 μM) in PBS (pH = 7.4);

Next, the binding affinity of these probes for Aβ aggregates was determined through a saturation binding assay according to conventional methods. As shown in table 1, probes **4** and **5** showed high affinity to $A\beta_{1\text{–}42}$ aggregates with the binding constant values of 28.2± 2 nM and 59.8±6 nM, respectively.

3.4. ADMET studies, biostability and effect of probes on cell viability in SH-SY5Y cells

ADMET studies were conducted to predict the hepatotoxicity, absorption and ability of BBB penetration. As anticipated, ADMET aqueous solubility levels of these new probes were 2 and 3, which are more soluble than compound 4a[30] (Table S1). Cytochrome P450 (CYP2D6) inhibition of these probes were classified as 0 and compound 4a as 1, indicating they are non-inhibitor of CYP2D6 and less toxic than the compound compound 4a. This suggested that potential adverse effects resulting from drug interaction upon administration of these probes are unlikely. Moreover, probes **4**, **5** and compound 4a were classed as 0 and 1 for human intestinal absorption (HIA) and blood brain barrier (BBB) shown in Table S1 and have fallen inside 99% human intestinal absorption confidence ellipsoid as well as the 99% BBB confidence ellipsoid (Figure S6), predicting that they are expected to posses high BBB penetration and good human intestinal absorption.

The plasma stability of probes and the cytotoxicity of these probes on human neuron cells are crucial requirements in vivo efficacy. We first examined the stability of our probes in mice plasma before in vivo imaging. As shown in Figure S7, nearly 99% of these probes remained after 30/60 min incubation at 37 °C, indicating that they are stable in mice plasma. Then, we assessed by using a MTT assay the viability of human neuroblastoma cells (SH-

SY5Y) with or without exposure to light in the culture medium. As shown in Figure 3, there was no significant cytotoxicity observed at a concentration of 50 μM.

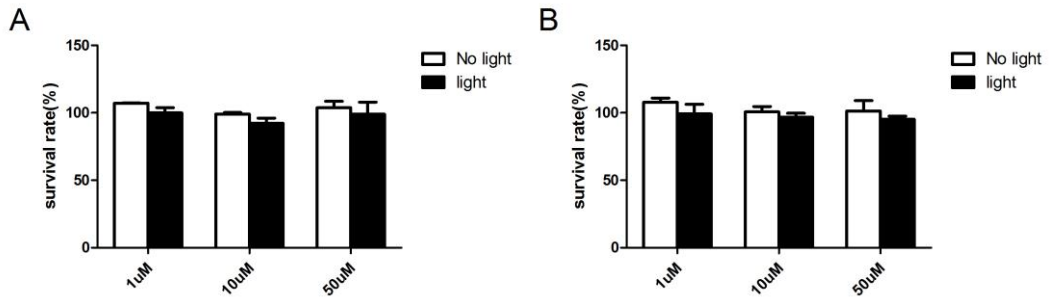

Figure 3. Cell viability after incubation of **4** (A) or **5** (B) at different concentrations (1, 10 and 50 μM) with a human neuronal cell line (SH-SY5Y) by MTT assay, at 37°C for 24 h with or without exposure to light.

3.5. In vivo imaging and ex vivo fluorescence staining

To validate the potential of probe **4** for specific β–amyloid plaque imaging in vivo, in the brain double transgenic mice (C57BL/6, APP/PS1, 12 months old, male) and age-matched wild mice (C57BL/6, 12 months old, male) were used. Fluorescence signals of the brain were recorded and compared at different time points (0-60 min) with the mice anesthetized and intravenously injected with probe **4** (4 mg/kg, 20% DMSO, 80% propylene glycol, 50 μL). As shown in Figure 5, the fluorescence intensity from the brains of Tg mice were significantly higher than that from the age matched WT mice at the same post-injection time point of 5-60 min, suggesting that probe **4** could efficiently penetrate the BBB and detect Aβ plaques in vivo.

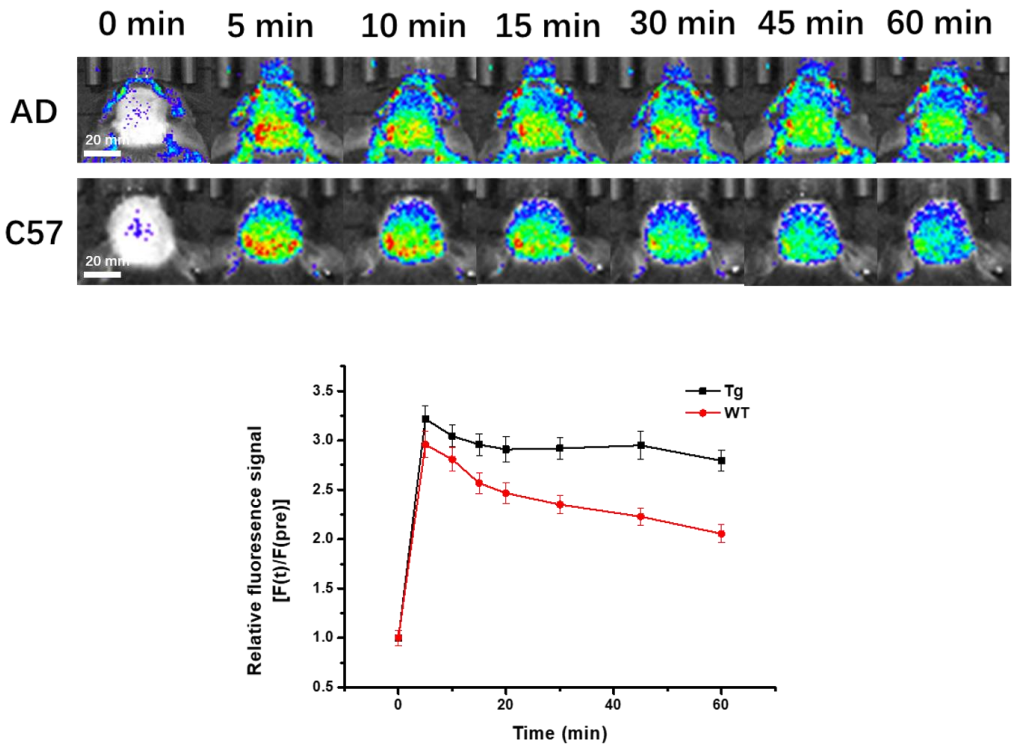

Figure 4. In vivo imaging study with probe **4**. (A) Fluorescence images of the same Tg (top row) and WT (bottom row) mouse head at selected time points before or after i.v. injection. (B) The relative fluorescence signal [F(t)/F(pre)] in the brain regions of Tg and WT mice after iv injection.

To further confirm the binding of probe **4** to Aβ fibrils in vivo, ex vivo histology was performed in Tg mice and wild-type control mice. After iv injection of **4**, Aβ plaques were clearly observed in the brain slices from Tg mice (Figure 5A), which is further verified by staining the same section with ThT, a standard staining used for Aβ plaques (Figure 5B). As expected, no plaques were found on the brain slices from the WT mouse (Figure 5B and 5E). These results were well consistent with that observed with fluorescence staining of probe **4** on brain slices in the cortex region (Figure S5B) and hippocampus region (Figure S5H) from a double Tg mouse and WT mice, indicating that probe **4** can label β-amyloid plaque in the brain slice.

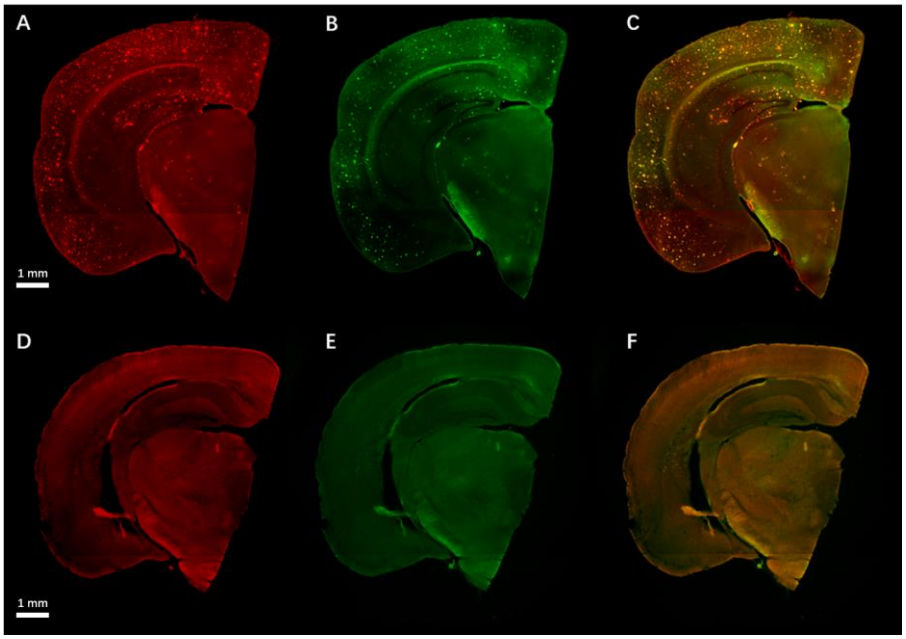

Figure 5. Ex vivo histology staining of brain slices from a Tg mouse (A) and wild-type control mouse (D) after injection of probe **4**. The Aβ plaques were further confirmed by staining the same sections with ThT (B, E). Graphical representation of overlap for fluorescence labeling by probe **4** and ThT (C, F)

3.6. Inhibitory effect of probes toward Aβ aggregation

To investigate their therapeutic potentials, we first carried out an in vitro $A\beta_{1-42}$ aggregation assay as previously reported.[30] Curcumin, a natural product was demonstrated to inhibit the formation of amyloid fibrils as well as their precursor oligomers and to reduce amyloid deposition in vivo.[35] In this assay, it was used as a control and shown to inhibit $A\beta_{1-42}$ aggregation with IC_{50} value of 16.4 μM. It is worth noting that our probes **4** and **5** exhibited higher inhibitory activities with an IC_{50} value of 0.4 μM and 0.8 μM respectively, in compared with Curcumin.

Next, probe **4** was used to investigate its inhibition of intracellular self-aggregation of $A\beta_{1-42}$ in SH-SY5Y cells by using fluorescence microscopy. In accordance with the in vitro Aβ aggregate inhibition results, probe **4** displayed a similar inhibitory activity, which could be visualized under the fluorescence microscope shown in Figure 6.

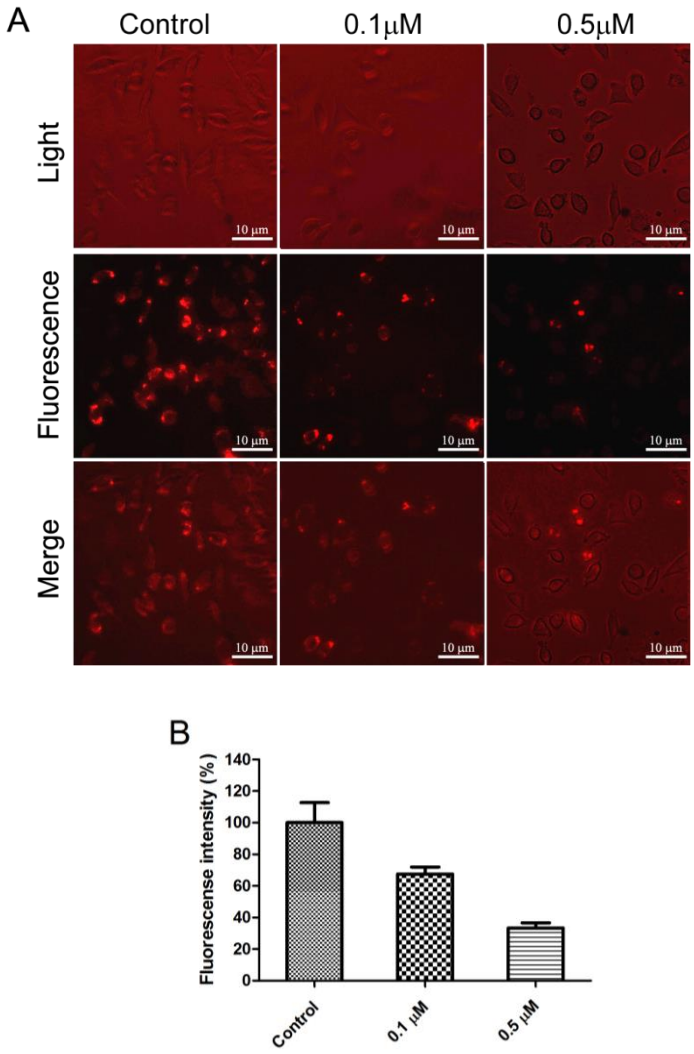

Figure 6. Inhibition of intracellular self-aggregation of $A\beta_{1\text{-}42}$ in SH-SY5Y cell line. Cells grown in the presence of Aβ monomer and probe **4** (0, 0.1 and 0.5 μM) for 2 days. For control experiment, probe **4** was added after 2 days without treatment, then imaged using fluorescence microscopy (A, magnification: 5X). Fluorescent were quantified and reported to the number of cells (B). Error bars, s.e.m from three independent experiments and four random fields.

3.7. Effect of probes against $A\beta_{1\text{-}42}$-induced human neuroblastoma cell toxicity

To confirm the protective effect of our probes on $A\beta_{1\text{–}42}$-induced toxicity, we measured the viability of SHSY5Y cells by MTT assay. As shown in Figure 7, $A\beta_{1\text{-}42}$ treatment significantly increased cytotoxicity compared with the control. As expected, different concentrations of probes **4**, **5** or curcumin were applied to with monomeric $A\beta_{1\text{-}42}$ at a concentration of 5 μM in SHSY5Y cell line resulted in the increase of cell viability in a

dose-dependent manner. Moreover, in comparison with curcumin, our probes showed a stronger protective effect on the toxicity of SHSY5Y cells induced by $A\beta_{1-42}$.

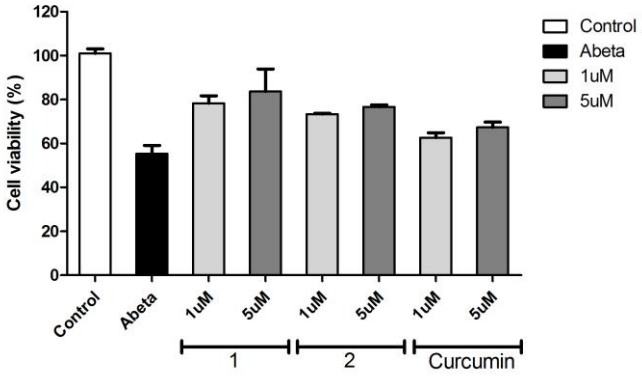

Figure 7. The protective effect of probes **4** and **5** or curcumin against the toxicity induced by $A\beta_{1-42}$.

3.8. Docking studies

Molecular docking is a strong research tool in studying protein-ligand interactions, due to its ability to predict the binding-conformation of small molecule ligands to the appropriate target binding site with respect to that experimentally observed. Such methods have been also used in exploring the binding modes and interactions of fluorescent probes with Aβ.[36] In this study, the binding nature of our probes to the fibrils was investigated by docking simulation. As shown in Figure S8, probes **4** and **5** could bind to the grooves on the KLVFFA fibril surface, un identical binding site to Congo Red, used for staining in amyloidosis.[37] Our probes occupied a binding site formed by the nonpolar residues Val18 and Phe20, which was dominated by hydrophobic interactions. Hydrogen bonds which played an important role in the dock conformations of the probes were also observed between probes and Lys16 that formed an another site with Val18 at the surface of the fibril. In addition, the experimental Kd values correlated well with the calculated binding energies of compound 4a1 (-8.76 Kcal/mol), **4** (-8.63 Kcal/mol) and **5** (-8.05 Kcal/mol) with Aβ fibrils. Compound 4a1 had a higher affinity (7.5 ± 0.4 nM)[30] than those of **4** (Kd = 28.2 nM) and **5** (Kd = 59.8 nM). This was probably due to larger steric hindrance of probes **4** and **5**, which resulted in a weaker hydrophobic interaction with Val18 and Phe20.

4. Conclusion

In this report, a systematic evaluation of novel phenothiazine-based theranostic agents was performed including fluorescent spectroscopic properties, in vitro evaluations, Aβ aggregate inhibition, protective effects on the toxicity of SHSY5Y cells induced by $A\beta_{1-42}$ and in vivo NIR imaging. These smart probes had high sensitivity and good fluorescent property changes upon binding to Aβ aggregates, possessed a good stability in mice plasma, BBB permeability and low cytotoxicity in SH-SY5Y cells as well as displayed a high binding affinity toward Aβ species. Remarkably, probe **4** performed excellent in vivo imaging of β-amyloid plaques, prevent self-aggregation of Aβ monomer from forming toxic oligmers and show a significantly beneficial effect on the toxicity of human neuroblastoma cells induced by $A\beta_{1-42}$. Furthermore, molecular docking provided insight into the mode of binding of our probes with the Aβ fibrils. In summary, our findings make this type of probes a robust and promising theranostic agents for basic research and potential clinic applications in AD.

Author information

// Y.L., J. C. and L.Y. contributed equally to this work.

Notes

The authors declare no competing financial interest.

Acknowledgements

We would like to thank China Science Foundation (grant no. 21672043) for financial support.

References

[1] Giacobini E, Gold G. Alzheimer disease therapy--moving from amyloid-β to tau. Nat. Rev. Neurol. 2013; 9: 677–686.

[2] Selkoe D. Resolving controversies on the path to Alzheimer's therapeutics. J. Nat. Med. 2011; 17: 1060–1065.

[3] Buckholtz NS, Ryan LM, Petanceska S, Refolo LM. NIA commentary: translational issues in Alzheimer's disease drug development. Neuropsychopharmacology 2012; 37: 284–286.

[4] Mishra P, Ayyannan SR, Panda G. Perspectives on Inhibiting β-Amyloid Aggregation through Structure-Based Drug Design. ChemMedChem 2015; 10: 1467–1474.

[5] Cho JE, Kim JR. Recent approaches targeting beta-amyloid for therapeutic intervention of Alzheimer's disease. Recent Patents CNS Drug Discov. 2011; 6: 222–233.

[6] Chen X, Yan SD. Mitochondrial Abeta: a potential cause of metabolic dysfunction in Alzheimer's disease. IUBMB Life 2006; 58: 686–694.

[7] Bitan G, Kirkitadze MD, Lomakin A, Vollers SS, Benedek GB, Teplow DB. Amyloid beta -protein (Abeta) assembly: Abeta 40 and Abeta 42 oligomerize through distinct pathways. Proc Natl. Acad. Sci. US A 2003; 100: 330–335.

[8] Nie Q, Du X, Geng M. Small molecule inhibitors of amyloid β peptide aggregation as a potential therapeutic strategy for Alzheimer's disease. Acta Pharmacol. Sin. 2011; 32: 545–551.

[9] Upadhaya A R, Kosterin I, Kumar S, von Arnim CA, Yamaguchi H, Fandrich M, Walter J, Thal DR. Biochemical stages of amyloid-β peptide aggregation and accumulation in the human brain and their association with symptomatic and pathologically preclinical Alzheimer's disease. Brain 2014; 137: 887–903.

[10] Jin M., Shepardson N, Yang T, Chen G, Walsh D, Selkoe DJ. Soluble amyloid beta-protein dimers isolated from Alzheimer cortex directly induce Tau hyperphosphorylation and neuritic degeneration. Proc. Natl. Acad. Sci. USA 2011; 108: 5819–5824.

[11] Rowan MJ, Klyubin I, Wang, Q, Hu NW. Anwyl, R. Synaptic memory mechanisms: Alzheimer's disease amyloid beta-peptide-induced dysfunction. Biochem. Soc. Trans 2007; 35: 1219–1223.

[12] Hu NW, Smith IM, Walsh DM, Rowan MJ. Soluble amyloid-beta peptides potently disrupt hippocampal synaptic plasticity in the absence of cerebrovascular dysfunction in vivo. Brain J. Neurol. 2008; 131: 2414–2424.

[13] Reddy PH, Beal MF. Amyloid beta, mitochondrial dysfunction and synaptic damage: implications for cognitive decline in aging and Alzheimer's disease. Trends Mol. Med. 2008; 14: 45–53.

[14] Ruan L, Kang Z, Pei G, Le Y. Amyloid deposition and inflammation in APPswe/PS1dE9 mouse model of Alzheimer's disease. Curr. Alzheimer Res. 2009; 6: 531–540.

[15] Uttara B, Singh AV, Zamboni P, Mahajan R. Oxidative stress and neurodegenerative diseases: a review of upstream and downstream antioxidant therapeutic options. Curr. Neuropharmacol. 2009; 7: 65–74.

[16] Brzyska M, Elbaum D, Dysregulation of calcium in Alzheimer's disease. Acta Neurobiol. Exp. 2003; 63: 171–183.

[17] Bolognesi ML. in Medicinal Chemistry Approaches to Personalized Medicine, K. Lackey and B. D. Roth, Wiley-VCH, 2013, ch. 9.

[18] Holtzman DM, Morris JC, Goate AM. Alzheimer's disease: the challenge of the second century. Sci. Transl. Med. 2011; 3: 77sr1.

[19] Hardy J, Selkoe DJ. The amyloid hypothesis of Alzheimer's disease: progress and problems on the road to therapeutics. Science, 2002; 297: 353–356.

[20] Chen G.F, Xu TH, Yan Y, Zhou YR, Jiang Y, Melcher K, Xu HE. Amyloid beta: structure, biology and structure-based therapeutic development. Acta Pharmacol. Sin. 2017; 38: 1205–1235

[21] Han X, He G. Toward a Rational Design to Regulate β-Amyloid Fibrillation for Alzheimer's Disease Treatment. ACS Chem. Neurosci. 2018; 9: 198–210.

[22] Sarantopoulos A, Beziere N, Ntziachristos V. Optical and opto-acoustic interventional imaging. Ann. Biomed. Eng. 2012; 40: 346–366.

[23] Stuker F, Ripol J, Rudin M. Fluorescence molecular tomography: principles and potential for pharmaceutical research. Pharmaceutics 2011; 3: 229–274.

[24] Hintersteiner M, Enz A, Frey P, Jaton A.L, Kinzy W, Kneuer R, Neumann U, Rudin M, Staufenbiel M, Stoeckli M, Wiederhold KH, Gremlich HU. In vivo detection of amyloid-beta deposits by near-infrared imaging using an oxazine-derivative probe. Nat. Biotechnol. 2005; 23: 577−583.

[25] Nesterov EE, Skoch J, Hyman BT, Klunk WE, Bacskai BJ, Swager TM. In vivo optical imaging of amyloid aggregates in brain: design of fluorescent markers. Angew. Chem., Int. Ed., 2005; 44: 5452–5456.

[26] Ran C, Xu X, Raymond SB, Ferrara BJ, Neal K, Bacskai BJ, Medarova Z, Moore A. Design, synthesis, and testing of difluoroboron-derivatized curcumins as near-infrared probes for in vivo detection of amyloid-beta deposits. J. Am. Chem. Soc. 2009; 131: 15257–15261.

[27] Ono M, Watanabe H, Kimura H, Saji H. BODIPY-based molecular probe for imaging of cerebral β-amyloid plaques. ACS Chem. Neurosci. 2012; 3: 319−324.

[28] Schmidt A, Pahnke J. Efficient near-infrared in vivo imaging of amyoid-β deposits in Alzheimer's disease mouse models. J. Alzheimer's Dis., 2012; 30: 651−664.

[29] Cui M, Ono M, Watanabe H, Kimura H, Liu B, Saji H. Smart near-infrared fluorescence probes with donor-acceptor structure for in vivo detection of β-amyloid deposits. J. Am. Chem. Soc., 2014; 136: 3388−3394.

[30] Dao P, Ye FF, Liu Y, Du ZY, Zhang K, Dong CZ, Meunier B, Chen H. Development of Phenothiazine-Based Theranostic Compounds That Act Both as Inhibitors of β-Amyloid Aggregation and as Imaging Probes for Amyloid Plaques in Alzheimer's Disease. ACS Chem. Neurosci. 2017; 8: 798–806.

[31] Clark M, Cramer RD, Opdenbosch NV. Validation of the general purpose tripos 5.2 force field. Journal of Computational Chemistry 1989; 10: 982–1012.

[32] Gasteiger J, Marsili M. Polarisation nucleaire induite chimiquement: etude comparative de la decomposition thermique et photochimique de peroxydes d'acyle benzoyle. Tetrahedron 1979; 36: 3219–3228.

[33] Marsili M, Gasteige, J. Charge Distribution from Molecular Topology and Orbital Electronegativity. Croatica Chemica ACTA 1980; 53: 601–614.

[34] Cook NP, Ozbil M, Katsampes C, Prabhakar R, Marti AA. Unraveling the photoluminescence response of light-switching ruthenium(II) complexes bound to amyloid-β. J. Am. Chem. Soc. 2013; 135: 10810–10816.

[35] Yang F, Lim GP, Begum AN, Ubeda OJ, Simmons MR, Ambegaokar SS, Chen P, Kayed R, Glabe CG, Frautschy SA, Cole GM. Curcumin inhibits formation of amyloid beta oligomers and fibrils, binds plaques, and reduces amyloid in vivo. J. Bio. Chem. 2005; 280: 5892–5901.

[36] Wu C, Scott J, Shea JM. Binding of Congo red to amyloid protofibrils of the Alzheimer Aβ(9-40) peptide probed by molecular dynamics simulations. Biophys. J. 2012; 103: 550–557.

[37] Wu C, Wang Z, Lei H, Zhang W, Duan Y. Dual binding modes of Congo red to amyloid protofibril surface observed in molecular dynamics simulations. J. Am. Chem. Soc. 2007; 129: 1225–1232.

Phenothiazine-based theranostic compounds for in vivo near-infared fluorescence imaging of β-amyloid plaques and inhibition of Ab aggregation

YongLiang Li, Jing Cai, Longjia Yan, Wanzheng Zhang, Le Li, Zhiyun Du, Yan XiongFang, ChangZhi Dong, Bernard Meunier, Huixiong Chen

NIR Fluorophores

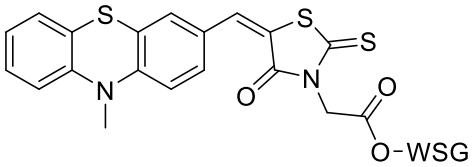

WSG = Water Solubilizing Group